Targetable conformationally restricted cyanines enable photon-count limited applications

Patrick Eiring,[a] ‡ Ryan McLaughlin,[b] ‡ Siddharth S. Matikonda,[b] ‡ Zhongying Han,[c] ‡ Lennart Grabenhorst,[d] Dominic A. Helmerich,[a] Mara Meub,[a] Gerti Beliu,[a] Michael Luciano,[b] Venu Bandi,[b] Niels Zijlstra,[d] Zhen-Dan Shi,[e] Rolf Swenson,[e] Philip Tinnefeld,[d] Viktorija Glembockyte,*[d] Thorben Cordes,*[c] Markus Sauer*[a] and Martin J. Schnermann*[b]

[a] P. Eiring, D. A. Helmerich, M. Meub, Dr. Gerti Beliu, Prof. Dr. M. Sauer*
Department of Biotechnology and Biophysics Biocenter
Julius-Maximilians-Universität Würzburg
Am Hubland, 97074 Würzburg, Germany
E-mail: m.sauer@uni-wuerzburg.de

[b] R. McLaughlin, Dr. S. Matikonda, Dr. M. Luciano, Dr. V. Bandi, Dr. M. J. Schnermann*
Laboratory of Chemical Biology
Center for Cancer Research, National Cancer Institute
Frederick, Maryland 21702, USA
E-mail: martin.schnermann@nih.gov

[c] Msc. Zhongying Han, Dr. Niels Zijlstra, Prof. Dr. T. Cordes,
Physical and Synthetic Biology, Faculty of Biology, Ludwig-Maximilians-Universität München,
Großhadernerstr. 2-4 82152 Planegg-Martinsried, Germany,
E-mail: cordes@bio.lmu.de

[d] L. Grabenhorst, Prof. Dr. Philip Tinnefeld, Dr. V. Glembockyte*
Department of Chemistry and Center for NanoScience
Ludwig-Maximilians-Universität München
Butenandtstr. 5-13, 81377 München, Germany
E-mail: v.glembockyte@lmu.de

[e] Dr. Z.H. Shen, Dr. R. Swenson
Chemistry and Synthesis Center
National Heart, Lung, and Blood Institute, NIH
Rockville, MD 20850, USA

‡ These co-authors contributed equally

Supporting information for this article is given via a link at the end of the document.

Abstract: Cyanine dyes are exceptionally useful probes for a range of fluorescence-based applications. We recently demonstrated that appending a ring system to the pentamethine cyanine ring system improves the quantum yield and extends the fluorescence lifetime. Here, we report an optimized synthesis of persulfonated variants that enable efficient labeling of nucleic acids and proteins. We demonstrate that a bifunctional sulfonated tertiary amide significantly improves the optical properties of the resulting bioconjugates. These new conformationally restricted cyanines are compared to parent species in a range of contexts including their use on a DNA-nano-antenna, in single-molecule Förster resonance energy transfer (FRET) applications, far-red fluorescence lifetime imaging microscopy (FLIM), and single-molecule localization microscopy. These efforts define contexts in which eliminating cyanine isomerization provides meaningful benefits to imaging performance.

Modern fluorescence-based methods put intense demands on fluorescent probes.[1-5] Cyanine dyes, especially the pentamethine cyanines Cy5 and Alexa Fluor 647, are invaluable probes in a range of contexts, despite modest quantum yields.[7] We recently introduced the novel pentamethine cyanine Cy5B where excited-state trans-to-cis photoisomerization is blocked by installation of a conformationally restraining ring system.[6] Relative to conventional cyanines, these compounds exhibit improved fluorescence quantum yield and longer fluorescence lifetimes. Small molecule conjugates underwent efficient recovery from hydride reduction (reductive caging) to enable high quality single-molecule localization microscopy (SMLM) in oxygenated buffer.[7] However, immunofluorescent and other biomolecule targeted applications were not possible due to the propensity of these compounds to form non-fluorescent aggregates. Here we report the optimized synthesis of di-sulfonated and tri-sulfonated derivatives and detail the application of these probes in several settings.

The physical properties of fluorescent probes is crucial to the advanced imaging applications, and sulfonation is an exceptionally versatile strategy in this context.[8-11] Scheme 1 details the synthesis of di- and tri-sulfonated conformationally restrained pentamethine cyanines. Indolinine **3**, bearing a functionalizable methyl ester, was accessed through Fisher indole synthesis and alkylation from **1**. Similar to prior efforts, we found that conventional cyanine formation with **3** and previously reported **4** afforded the desired mixed cyanine in modest yield (14%) after a complex purification process.[13] Consequently, we then examined alternative approaches to unsymmetrical cyanine formation, as several have been reported.[14-

Scheme 1: Synthesis of Cy5B-disulfo and -trisulfo NHS Esters.

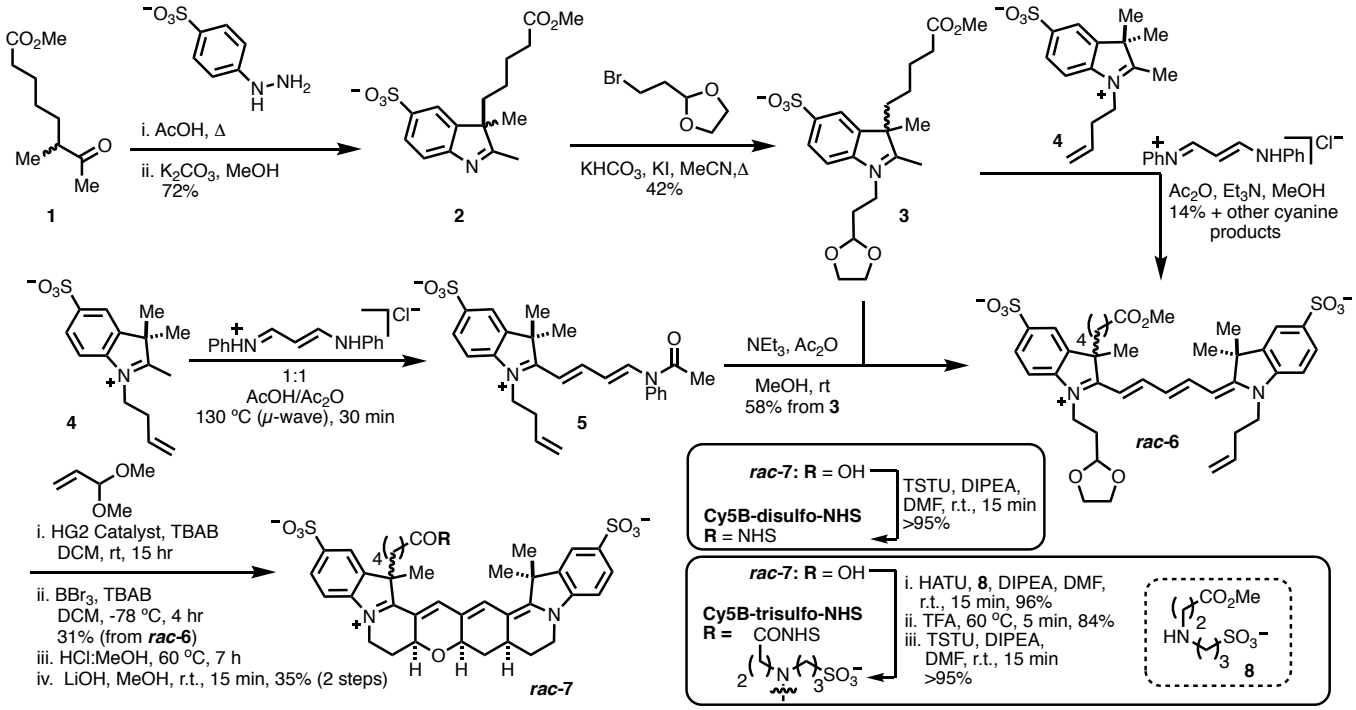

[17] Notably, solid phase methods proved difficult to implement on significant scale. By contrast, a solution-phase sequential heterocycle addition sequence, based on a report by Wolf and coworkers, provide scalable reproducible access to ***rac*-6** on up to gram scales.[14] This approach involved addition of **4** to the cyanine precursor, malonaldehyde bis(phenylimine) monohydrochloride, with microwave irradiation (130 ˚C, 30 min) to first form acylated hemicyanine **5**. This unpurified intermediate was then reacted with **3** at r.t. to provide unsymmetrical pentamethine cyanine ***rac*-6**, in good yield (58% from **3**) with only trace formation of other cyanine products. While installation of the α–β unsaturated aldehyde via cross-metathesis reaction was unsuccessful initially due to the poor solubility of **3** in organic solvent, we ultimately found that the addition of a phase transfer catalyst, tetrabutylammonium bromide, enabled the reaction to proceed efficiently. The key tetracyclization reaction was carried out using BBr_3 in CH_2Cl_2, again with tetrabutylammonium bromide acting as a critical solubility-enhancing additive. As observed previously,[6] the initial cyclization reaction formed a mixture of diastereomers which were equilibrated using protic acidic conditions to form the *syn* product ***rac*-7**, which is a mixture of diastereomers around the pyran ring due to the additional chiral center. The mixture ***rac*-7** could be converted to the corresponding NHS-ester, Cy5B-disulfo-NHS, through a saponification/TSTU sequence. Alternatively, the tertiary amide, Cy5B-trisulfo-NHS, could be formed via saponification and coupling with amine **8**, followed by saponification/TSTU NHS-ester formation.

We then assessed the optical properties of these compounds, as well as their antibody conjugates (Table 1). As a comparison, we used a disulfonated pentamethine cyanine (Cy5).[18] As free dyes, both conformationally restrained dyes Cy5B-disulfo and Cy5B-trisulfo have higher quantum yield (Φ_F) and longer fluorescence lifetimes (τ_F) as Cy5, albeit with moderately reduced extinction coefficients (ε) in an aqueous environment (Table 1). These values are quite similar to the monosulfonated derivative we

Table 1. Spectroscopic characteristics of free dyes and mAB conjugates in PBS, pH 7.4, and MeOH:PBS (1:1). n.d. = not determined.

A. Free Dyes

Solvent	λ_{max} (nm)	ε ($M^{-1}cm^{-1}$)	λ_{em} (nm)	Φ_F	τ_F (ns)
Cy5					
PBS	647	270,000	665	0.26	1.09
PBS:MeOH	648	279,000	670	n.d.	n.d.
Cy5B-Disulfo					
PBS	669	193,000	684	0.45	1.89
PBS:MeOH	671	227,000	687	n.d.	n.d.
Cy5B-Trisulfo					
PBS	669	241,000	685	0.40	1.85
PBS:MeOH	671	278,000	688	n.d.	n.d.

B. mAb-Dye Conjugates

Construct	Φ_F	$\frac{\Phi_F \text{ - labeled}}{\Phi_F \text{ - free dye}}$	τ_F (ns)	$\frac{\tau_F \text{ - labeled}}{\tau_F \text{ - free dye}}$
DOL-1				
Cy5-mAb	0.21	0.81	1.53	1.41
Cy5B-Disulfo- mAb	0.38	0.84	2.08	1.10
Cy5B-Trisulfo- mAb	0.41	1.03	2.13	1.15
DOL-3				
Cy5-mAb	0.11	0.42	1.22	1.12
Cy5B-Disulfo- mAb	0.31	0.69	1.79	0.95
Cy5B-Trisulfo- mAb	0.39	0.98	2.21	1.19

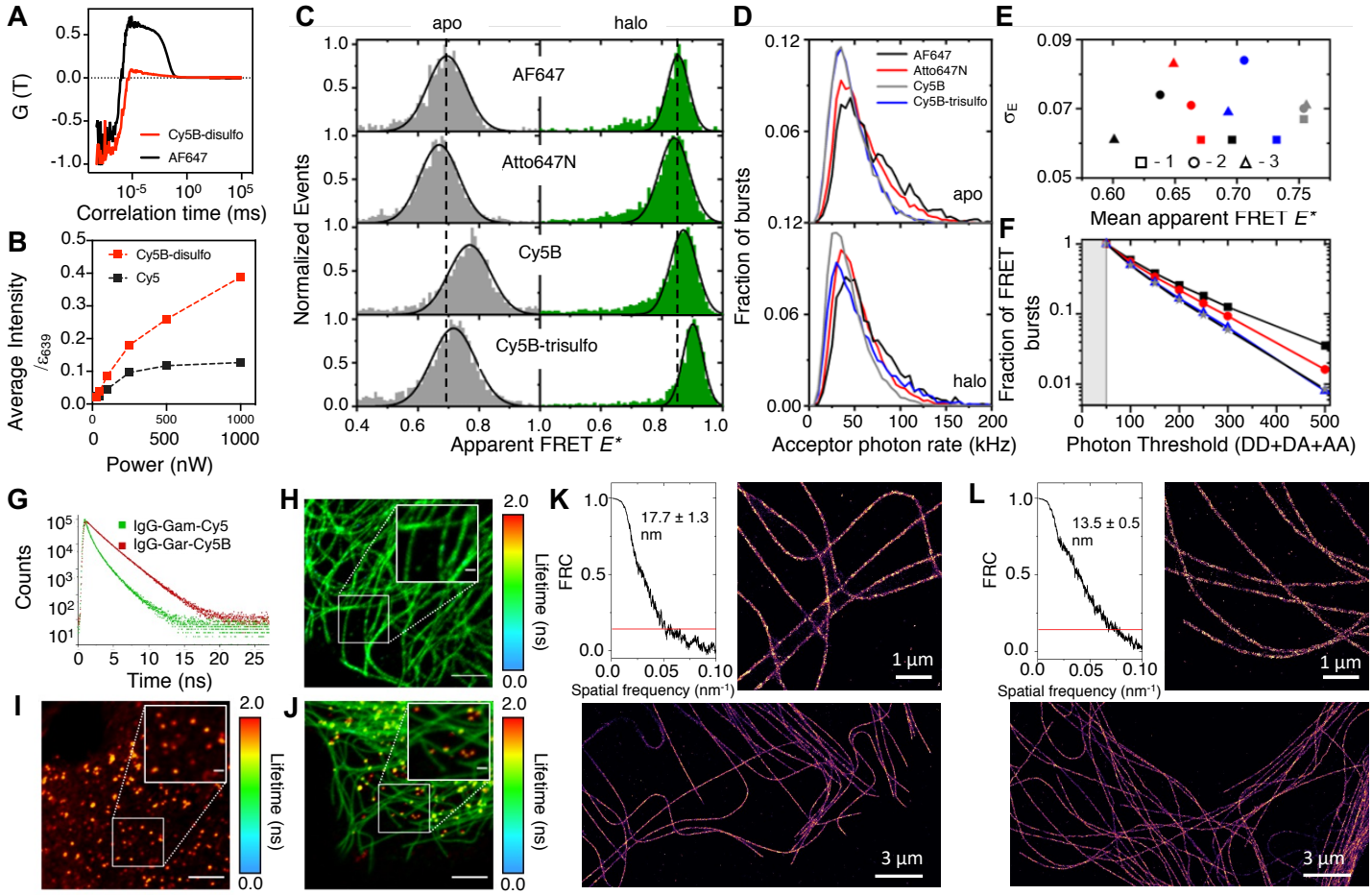

Figure 1. (A) Average autocorrelation of fluorescence signal obtained from single Cy5B-disulfo and AF647 molecules (33 and 37 molecules, respectively) immobilized on a glass slide via DNA origami nanostructures and excited at 639 nm in the presence of ROXS and in the absence of oxygen. (B) Average intensity of single Cy5B-disulfo and AF647 in the hotspot of DNA nanoantennas obtained at increasing excitation intensities. The fluorescence intensities of single molecules were normalized to the extinction coefficient at the excitation wavelength (639 nm). Saturation in fluorescence intensity is more pronounced for AF647 presumably due to the trans-cis photoisomerization process which does not occur Cy5B-disulfo. (C) Apparent FRET efficiency E* histograms of MalE variant T36C/S352C obtained from single-molecule FRET experiments of freely diffusing proteins in a confocal microscope. The MalE double cysteine variant was labeled with donor fluorophore AF555 and different FRET acceptor fluorophores as indicated in the figure panels (AF647, ATTO647N, Cy5B, and Cy5B-trisulfo) and purified via size-exclusion chromatography to remove unbound dye (Figure S1). E* histograms were recorded in the absence (*apo*) and presence of saturating ligand concentrations of 100 µM maltose (holo). Solid lines are the projections of 2D Gaussian fits to the data from which the mean apparent FRET efficiency and width of the histogram was determined (see panel E). All histograms were recorded using microsecond alternating laser excitation (ALEX) with excitation powers of 60 µW at 532 nm and 25 µW at 640 nm. The data was analyzed using an all photon burst search with an additional threshold on DD+DA+AA of 150. All histograms shown are projections from bursts with a stoichiometry between 0.3 and 0.7. Full data sets of all conditions plotted (including intermediate ligand concentrations) are shown in Figure S2 & S3. (D) Photon counting histograms (PCH) of the same data sets as in (C) obtained from direct acceptor excitation for the protein in the apo and holo state. Only bursts with an apparent FRET efficiency of 0.4 - 1 and a stoichiometry between 0.3 and 0.8 were used for the analysis. The acceptor photon count rate was determined by comparison of absolute number of detected photons and the respective burst length. (E) Influence of excitation power on the mean apparent FRET efficiency E* and the width of the σ_E of the gaussian fit for the four dye combinations (full data sets in Figure S3, same color code as panel D). Three distinct excitation conditions were used, where the ratio of green-to-red laser intensity was kept constant. Dotted data points were obtained with excitation powers of 60 µW at 532 nm and 25 µW at 640 nm, circles with 120 µW at 532 nm and 50 µW at 640 nm, and triangles at 180 µW at 532 nm and 75 µW at 640 nm. All data was recorded in the apo state (absence of ligand). (F) Fraction of bursts with intermediate stoichiometry values where both donor and acceptor dye were present ("FRET bursts") as a function of increasing all photon threshold (DD = Donor emission after Donor excitation, DA = Acceptor emission after Donor excitation, AA = Acceptor emission after Acceptor excitation). The survival fraction of FRET bursts was normalized to the number of FRET bursts at a photon threshold of 50. All data were all recorded in the absence of ligand with excitation powers of 60 µW at 532 nm and 25 µW at 640 nm. The same colors were used as in panel D to indicate the different acceptor dyes. (G) Fluorescence decays of goat anti-rabbit IgG labeled with Cy5B-trisulfo (DOL 3.2) and goat anti-mouse IgG labeled with Cy5 (DOL 2) excited at 640 nm. The decays were measured at the emission maxima in PBS, pH 7.4. (H) FLIM image of a COS7 cell immunostained with mouse anti-ß-tubulin primary and goat anti-mouse secondary antibodies labeled with Cy5 (DOL 2). (I) FLIM image of a COS7 cell immunostained with rabbit anti-clathrin primary and goat anti-rabbit secondary antibodies labeled with Cy5Bdisulfo (DOL 3.2). (J) FLIM composite image of a COS7 cell immunostained with mouse anti-ß-tubulin primary and rabbit anti-clathrin primary and corresponding secondary Cy5 and Cy5B-disulfo labeled antibodies. Scale bars, 5 µm and 1 µm (insets). Single-molecule localization microscopy (SMLM) images of microtubules in immunolabeled with Cy5 (K) in 100 mM MEA/PBS (pH = 7.5) and Cy5B-trisulfo (L) in 0.1% $NaBH_4$/PBS upon irradiation with 640 nm (2.5 kW/cm^2) using an integration time of 20 ms (total acquisition time 10 min). Scale bars, 3 µm and 1 µm (insets). Fourier ring correlation (FRC) analysis[12] estimated spatial resolutions of 17.7 ± 1.3 nm (s.d.) for Cy5 and 13.5 ± 0.5 nm for Cy5B-trisulfo.

reported previously.[6] We then prepared goat anti-mouse antibodies labeled on average with a degrees of labeling (DOL) of 1 and 3 using conventional NHS-ester labeling conditions (Fig. S1). Several observations emerge from the spectroscopic properties of the resulting conjugates. First, with unrestrained Cy5, Φ_F decreased substantially, i.e. from 0.21 to 0.11 for DOL 3.0 and τ_F decreased only slightly, which is in line with prior observations (Table 1).[18-19] With the Cy5B-disulfo-mAb conjugates, Φ_F is similar to the free dye, but moderately reduced (by 31%) at higher labeling density. By contrast, the trisulfo derivative, exhibits nearly identical Φ_F at both

labeling densities, and moderately increased fluorescence lifetimes. This results suggest that this simple amide modification strategy improves the properties of the resulting conjugates. Overall, these studies illustrate that cyanine conformational restraint, when combined with optimized sulfonation, can result in fluorophore antibody conjugates with excellent optical properties. To investigate the difference in photophysical properties of Cy5B-trisulfo and Alexa Fluor 647 (AF647), a Cy5 derivative with two additional sulfonate groups,[18] we employed fluorescence correlation spectroscopy (FCS) as an analytical tool for short-lived transient species. Using the well-established ROXS buffer[19] and appending both probes to DNA-origami structures (Fig. 1A), AF647 exhibits a dark state in the microsecond time scale, which is consistent with *trans-cis* isomerization reported previously.[20] By contrast, Cy5B-disulfo provides a stable fluorescence signal both in the millisecond and microsecond time regime. Of note, the residual autocorrelation term in the Cy5B-disulfo can be attributed to fast blinking not completely removed by ROXS[21] and is present in both samples.

The lack of the photoisomerization process not only provides a “cleaner” fluorescent signal up to the microsecond time range but also increases the overall brightness of the molecule, since the dark *cis*-state can no longer be populated. This becomes particularly relevant when excitation rates are very high, as observed in plasmonic nanostructures.[22] Therefore, we placed the fluorophores in the plasmonic hotspot formed by two 100 nm gold nanoparticles using DNA origami nano-antennas (Fig. S2)[23] and extracted spot-wise fluorescence intensity values from confocal microscopy scans. When plotted as a function of normalized excitation intensity, Cy5B-disulfo is significantly brighter than AF647 at all excitation intensities. While both samples show a degree of saturation,[24] Cy5B-disulfo starts saturating only at much higher excitation intensities (Fig. 1B). At 1 µW excitation intensity, Cy5B-disulfo is more that 3-fold brighter than AF647. These findings indicate that these probes are well suited for experiments requiring high temporal resolution (i.e. high excitation intensities)**.**[25]

Diffusion-based single-molecule FRET (smFRET) has become a key method to study the structural dynamics of biomacromolecules under realistic conditions,[26] yet dye performance can be severely impacted by photo-induced blinking (e.g., triplet-state formation or *trans-cis* isomerization) and irreversible photobleaching.[27] This limits various aspects of smFRET experiments including the quality of the resulting FRET efficiency histograms, temporal resolution and distance accuracy. We evaluated Cy5B and Cy5B-trisulfo dyes using microsecond alternating excitation (ALEX) with maltose binding protein as a model system (Figure 2C-F, Figure S3-S6). The conformationally restrained sulfonated cyanine dyes were benchmarked against the state-of-the-art dye combinations used in the smFRET field (AF555 with AF647 and ATTO647N). The protein model systems was an established double-cysteine variant of MalE (Thr36Cys-Ser352Cys) that allows to study the conformational changes of MalE via stochastic labelling with maleimide fluorophores (Figure S4, See SI for the synthesis of Cy5B-trisulfo maleimide).[28-30] The labelling positions were chosen such that the apo conformation (absence of maltose) displays lower FRET efficiency in comparison to the holo state (100 µM maltose) of the protein (Figure S5). All double-labeled MalE with AF555 as donor dye visualized the expected conformational changes upon addition of maltose (Figure 1C). This meant that the protein adopts the low FRET open conformation in the absence of ligand, which is altered into the closed-liganded conformation when 100 µM maltose were added. Due to the spectral similarity between the acceptor dyes, all dye-pairs showed similar, yet not identical, mean FRET efficiencies and width with overall high histogram quality. In all cases, we also found a similar response of the FRET assays upon addition of 1.5 µM maltose (fraction closed of 0.3-0.4), a concentration close to the dissociation constant K_d for the protein-substrate interaction (Figure S4, S5).[28] To further benchmark the quantitative performance of the dyes against each other, we compared their acceptor photon count rates at 60 µW green and 25 µW red laser excitation intensity. Strikingly, we found a maltose dependent fluorophore brightness, where all dyes were similarly bright in the holo state, yet the Cy5B dyes were slightly less bright (by 5-10 kHz) in comparison with AF647 and ATTO647N in the apo state (Figure 2D). This observation suggests that less FRET bursts are retained for AF555-Cy5B-monosulfo and AF555-Cy5B-trisulfo in comparison to other two fluorophore pairs (Figure 1F). Nevertheless, the Cy5B derivatives showed a unique advantage over both AF647 and ATTO647N (Figure 1E). Due to the absence of cis/trans isomerization (in comparison to AF647) we found in a laser power dependence in the experiments of the apo state (Figure 1E, Figure S6) that the Cy5B dye had strongly reduced bridge artifacts caused by the acceptor dye and retained the mean E* position and width s_E of the population over the range of excitation powers studied (Figure 1E).[30] Also Cy5-trisulfo had only a small change of mean peak position, yet substantial change of the population width, which was similar to ATTO647N. These observations establish Cy5B and Cy5B-trisulfo as a useful alternative to AF647 and ATTO647N, particular when the goal of an experiment is to maintain correct mean FRET efficiencies and reduced bleaching/blinking artefacts, e.g., when higher laser powers are required than usual.

Having established the utility of these probes for *in vitro* single-molecule applications, we evaluated them for cellular applications. We first asked if the difference in fluorescence lifetimes of the sulfonated Cy5B and Cy5 antibody conjugates could be used for two-color fluorescence lifetime imaging microscopy (FLIM).[31-33] We performed FLIM measurements of Cy5 immunolabeled β-tubulin and detected an average fluorescence lifetime of 0.91 ns (Fig. 1G-J), whereas cells immunolabeled solely for clathrin with Cy5B-trisulfo showed a fluorescence lifetime of ~1.75 ns (Figs. 1a,c) similar to the values measured in ensemble TCSPC experiments (Table 1). Notably, we were able to obtain composite FLIM images of COS7 cells immunolabeled with both dyes based on the different fluorescence lifetimes of Cy5 and Cy5B-trisulfo labeled antibodies (Fig. 1J).

Finally, we evaluated the performance of the new red-absorbing dyes in single-molecule localization microscopy (SMLM) experiments. We immunostained β-tubulin of COS7 cells with Cy5 and Cy5B-trisulfo, as this is a well-established reference structure, to investigate the spatial resolution of super-resolution microscopy methods. Microtubules are hollow tubes with an outer diameter of 25 nm and 60 nm, respectively, after immunostaining with primary and secondary antibodies.[34] *Direct* stochastic optical reconstruction microscopy (*d*STORM)[35] imaging of Cy5 (Fig. 1K) was performed in standard photoswitching buffer (100 mM MEA, pH 7.5, without enzymatic oxygen depletion whereas Cy5B-trisulfo was reduced over 30 min in $NaBH_4$/PBS and measured in the same buffer by TIRF microscopy using solely 640 nm irradiation (Fig. 1L). Removal of residual reductant $NaBH_4$ and imaging in PBS provided a similar image quality (Fig. S7). Additional irradiation at 405 nm did

not significantly change the SMLM image quality (Fig. S8). For both dyes, Cy5 and Cy5B-trisulfo we could reconstruct high quality super-resolved microtubule images but for Cy5B-trisulfo we detected twice as many photon counts per ON-event (~1.800) as for Cy5 (~770), which translates into localization precisions of 6.6±3.3 nm (s.d.) for Cy5B-trisulfo and 8.4±4.4 nm (s.d.) for Cy5.[36] Fourier ring correlation analysis[12] of microtubule SMLM images corroborated these numbers and provided spatial resolutions of ~13 nm for Cy5B-trisulfo and ~19 nm for Cy5.

In conclusion, we report the optimized synthesis of conformationally restricted di- and tri-sulfonated pentamethine cyanines and their evaluation in various experiments were photon count is crucial. As we have shown for bio-orthogonal labeling and small molecule conjugates, we now demonstrate that this strategy provides exceptionally bright protein conjugates. [6, 37] The unique properties of these probes enable single-molecule applications including high photon-fluxes in DNA nanoantennas, FRET, and SMLM experiments. Going forward, these results suggest the use constrained pentamethine cyanines for live SMLM-imaging as imaging is performed in thiol-free and deoxygenated PBS. Additionally, conjugation using labeling strategies to further exploit their enhanced brightness is of significant interest. Broadly, these studies provide a new set of well characterized far-red probes with utility in demanding fluorescence-based applications.

Acknowledgements

R.M, S.S.M., M.P.L., V.B. and M.J.S. were supported by the Intramural Research Program of the National Institutes of Health, National Cancer Institute, Center for Cancer Research. M.J.S. thanks Dr. Joseph Barchi, NCI-CCR, for NMR assistance and Dr. James Kelley, NCI-CCR, for mass spectrometric analysis. M.M., D.A.H., G.B. and M.S. thank the European Regional Development Fund (EFRE project “Center for Personalized Molecular Immunotherapy”) and the Deutsche Forschungsgemeinschaft (SFB/TR 240, project number 374031971, A07) for financial support. Z.H. is grateful for a CSC PhD scholarship and N.Z. thanks the Alexander von Humboldt foundation for a postdoctoral fellowship. Work in the lab of T.C. was funded by the European Commission (ERC-StG No. 638536 – SM-IMPORT). VG acknowledges the support from European Union’s Horizon 2020 research and innovation program under the Marie Skłodowska-Curie actions (grant agreement No. 840741) and the support by Humboldt Research Fellowships from the Alexander von Humboldt Foundation. PT thanks the Deutsche Forschungsgemeinschaft (excellence cluster e-conversion under Germany’s Excellence Strategy - EXC2089/1–390776260; Project-ID 201269156 – SFB1032).

Keywords: Fluorescent dyes • cyanine dyes • conformational restriction • single-molecule fluorescence spectroscopy • DNA-nanotechnology • super-resolution microscopy

References:

[1] M. Sauer, M. Heilemann, *Chemical reviews* **2017**, *117*, 7478-7509.
[2] J.H. Jett, R.A. Keller, J.C. Martin, B.L. Marrone, R.K. Moyzis, R.L. Ratliff, N.K. Seitzinger, E.B. Shera, C.C. Stewart, *Journal of biomolecular structure and dynamics* **1989**, *7*, 301-309.
[3] W.E. Moerner, L. Kador, *Physical review letters* **1989**, *62*, 2535.
[4] M. Orrit, J. Bernard, *Physical review letters* **1990**, *65*, 2716.
[5] E.B. Shera, N.K. Seitzinger, L.M. Davis, R.A. Keller, S.A. Soper, *Chemical Physics Letters* **1990**, *174*, 553-557.
[6] M.S. Michie, R. Gotz, C. Franke, M. Bowler, N. Kumari, V. Magidson, M. Levitus, J. Loncarek, M. Sauer, M.J. Schnermann, *J Am Chem Soc* **2017**, *139*, 12406-12409.
[7] F. Waldchen, J. Schlegel, R. Gotz, M. Luciano, M. Schnermann, S. Doose, M. Sauer, *Nat Commun* **2020**, *11*, 887.
[8] M. Levitus, S. Ranjit, *Quarterly reviews of biophysics* **2011**, *44*, 123.
[9] R.B. Mujumdar, L.A. Ernst, S.R. Mujumdar, C.J. Lewis, A.S. Waggoner, *Bioconjugate chemistry* **1993**, *4*, 105-111.
[10] M.P. Luciano, S.N. Crooke, S. Nourian, I. Dingle, R.R. Nani, G. Kline, N.L. Patel, C.M. Robinson, S. Difilippantonio, J.D. Kalen, M.G. Finn, M.J. Schnermann, *Acs Chem Biol* **2019**, *14*, 934-940.
[11] K. Sato, T. Nagaya, Y. Nakamura, T. Harada, R.R. Nani, J.B. Shaum, A.P. Gorka, I. Kim, C.H. Paik, P.L. Choyke, M.J. Schnermann, H. Kobayashi, *Mol Pharm* **2015**, *12*, 3303-3311.
[12] R.P. Nieuwenhuizen, K.A. Lidke, M. Bates, D.L. Puig, D. Grunwald, S. Stallinga, B. Rieger, *Nat Methods* **2013**, *10*, 557-562.
[13] R.B. Mujumdar, L.A. Ernst, S.R. Mujumdar, C.J. Lewis, A.S. Waggoner, *Bioconjug Chem* **1993**, *4*, 105-111.
[14] S.J. Mason, S. Balasubramanian, *Org Lett* **2002**, *4*, 4261-4264.
[15] S.J. Mason, J.L. Hake, J. Nairne, W.J. Cummins, S. Balasubramanian, *J Org Chem* **2005**, *70*, 2939-2949.
[16] D.S. Pisoni, L. Todeschini, A.C. Borges, C.L. Petzhold, F.S. Rodembusch, L.F. Campo, *J Org Chem* **2014**, *79*, 5511-5520.
[17] N. Wolf, L. Kersting, C. Herok, C. Mihm, J. Seibel, *J Org Chem* **2020**, *85*, 9751-9760.
[18] B.J. Harvey, M. Levitus, *Journal of fluorescence* **2009**, *19*, 443.
[19] H.J. Gruber, C.D. Hahn, G. Kada, C.K. Riener, G.S. Harms, W. Ahrer, T.G. Dax, H.-G. Knaus, *Bioconjugate chemistry* **2000**, *11*, 696-704.
[20] J. Widengren, P. Schwille, *The Journal of Physical Chemistry A* **2000**, *104*, 6416-6428.
[21] J. Vogelsang, R. Kasper, C. Steinhauer, B. Person, M. Heilemann, M. Sauer, P. Tinnefeld, *Angew Chem Int Ed Engl* **2008**, *47*, 5465-5469.
[22] P. Anger, P. Bharadwaj, L. Novotny, *Phys Rev Lett* **2006**, *96*, 113002.
[23] G.P. Acuna, F.M. Moller, P. Holzmeister, S. Beater, B. Lalkens, P. Tinnefeld, *Science* **2012**, *338*, 506-510.
[24] L. Grabenhorst, K. Trofymchuk, F. Steiner, V. Glembockyte, P. Tinnefeld, *Methods Appl Fluoresc* **2020**, *8*, 024003.
[25] H.S. Chung, W.A. Eaton, *Curr Opin Struct Biol* **2018**, *48*, 30-39.
[26] E. Lerner, T. Cordes, A. Ingargiola, Y. Alhadid, S. Chung, X. Michalet, S. Weiss, *Science* **2018**, *359*.
[27] B. Hellenkamp, S. Schmid, O. Doroshenko, O. Opanasyuk, R. Kühnemuth, S.R. Adariani, B. Ambrose, M. Aznauryan, A. Barth, V. Birkedal, *Nature methods* **2018**, *15*, 669-676.
[28] M. de Boer, G. Gouridis, R. Vietrov, S.L. Begg, G.K. Schuurman-Wolters, F. Husada, N. Eleftheriadis, B. Poolman, C.A. McDevitt, T. Cordes, *Elife* **2019**, *8*.
[29] E. Lerner, A. Barth, J. Hendrix, B. Ambrose, V. Birkedal, S.C. Blanchard, R. Borner, H. Sung Chung, T. Cordes, T.D. Craggs, A.A. Deniz, J. Diao, J. Fei, R.L. Gonzalez, I.V. Gopich, T. Ha, C.A. Hanke, G. Haran, N.S. Hatzakis, S. Hohng, S.C. Hong, T. Hugel, A. Ingargiola, C. Joo, A.N. Kapanidis, H.D. Kim, T. Laurence, N.K. Lee, T.H. Lee, E.A. Lemke, E. Margeat, J. Michaelis, X. Michalet, S. Myong, D. Nettels, T.O. Peulen, E. Ploetz, Y. Razvag, N.C. Robb, B. Schuler, H. Soleimaninejad, C. Tang, R. Vafabakhsh, D.C. Lamb, C.A. Seidel, S. Weiss, *Elife* **2021**, *10*.
[30] X. Kong, E. Nir, K. Hamadani, S. Weiss, *J Am Chem Soc* **2007**, *129*, 4643-4654.
[31] P.I. Bastiaens, A. Squire, *Trends Cell Biol* **1999**, *9*, 48-52.
[32] T. Niehorster, A. Loschberger, I. Gregor, B. Kramer, H.J. Rahn, M. Patting, F. Koberling, J. Enderlein, M. Sauer, *Nat Methods* **2016**, *13*, 257-262.
[33] D.A. Helmerich, G. Beliu, M. Sauer, *Acs Nano* **2020**, *14*, 12629-12641.
[34] K. Weber, P.C. Rathke, M. Osborn, *Proc Natl Acad Sci U S A* **1978**, *75*, 1820-1824.
[35] M. Heilemann, S. van de Linde, M. Schuttpelz, R. Kasper, B. Seefeldt, A. Mukherjee, P. Tinnefeld, M. Sauer, *Angewandte Chemie* **2008**, *47*, 6172-6176.
[36] K.I. Mortensen, L.S. Churchman, J.A. Spudich, H. Flyvbjerg, *Nat Methods* **2010**, *7*, 377-381.
[37] G. Beliu, A.J. Kurz, A.C. Kuhlemann, L. Behringer-Pliess, M. Meub, N. Wolf, J. Seibel, Z.D. Shi, M. Schnermann, J.B. Grimm, L.D. Lavis, S. Doose, M. Sauer, *Commun Biol* **2019**, *2*, 261.